

Review

On-Chip Supercontinuum Generation Pumped by Short Wavelength Fiber Lasers

Peng Chen ¹, Zhe Long ¹, Qi Cheng ¹, Maozhuang Song ¹, Wei Wang ¹, Ruixue Liu ¹, Zheng Zhang ¹, Kai Xia ¹, Zhen Yang ², Lei Qian ¹, Shengchuang Bai ¹, Xunsi Wang ¹ , Peilong Yang ¹, Peipeng Xu ³, El Sayed Yousef ⁴ and Rongping Wang ^{1,*} 

- ¹ Laboratory of Infrared Material and Devices, Advanced Technology Research Institute, Ningbo University, Ningbo 315211, China; baishengchuang@nbu.edu.cn (S.B.)
² Suzhou Institute of Nano-Tech and Nano-Bionics, Chinese Academy of Sciences, Suzhou 215123, China
³ State Key Laboratory of Materials for Integrated Circuits, Shanghai Institute of Microsystem and Information Technology, Chinese Academy of Sciences, Shanghai 200050, China
⁴ Central Labs, King Khalid University, AlQura'a, Abha P.O. Box 906, Saudi Arabia; ayousf@kku.edu.sa
* Correspondence: wangrongping@nbu.edu.cn

Abstract: Supercontinuum (SC) generation pumped by fiber lasers with short wavelengths below 2.0 μm is important since it can provide a compact light source for various applications. We review the progress of SC generation in various materials regarding the formation of the waveguides and point out the existing issues in the current investigations and possible solutions in the future.

Keywords: supercontinuum; waveguide; short wavelength fiber laser

1. Introduction

The supercontinuum (SC) is a kind of broad spectrum that is excited by a pulsed laser in the nonlinear medium via various nonlinear mechanisms, including self-phase modulation (SPM), stimulated Raman scattering (SRS), soliton fission, optical wave breaking, four-wave mixing (FWM) and cross-phase modulation, along with the dispersion properties of the medium [1–5]. The brightness of the SC as a light source is several orders of magnitude higher than that of the synchrotron, but the whole facility to generate SC is much cheaper, and thus, such a broad SC source can find its various applications in optical tomography, fluorescence microscopy, spectroscopy, and molecular sensing [5]. Usually, the SC spectrum from a nonlinear medium can be maximumly expanded via the dispersive engineering of the waveguide structure, e.g., using a pump wavelength close to the zero dispersive wavelength (ZDW), which can be finely tuned via careful structural design in the waveguide.

Various pump sources have been used to generate SC, and the dominant pump sources are the optical parametric oscillator (OPO)/optical parametric amplifier (OPA) systems and the all-solid-state lasers [4,5]. They have several advantages, like high peak power, ultra-short pulse duration, excellent beam quality, and a high spectral contrast ratio. However, the former is usually expensive, with large footprints and low robustness, while the latter is a promising alternative due to its high brightness, compact structure, good beam quality, high stability, and cost-effectiveness. In particular, fiber lasers are well-suited for meeting the requirements of low average power and high compactness, as the fibers used in these experiments can be spooled to a centimeter-scale ring with negligible bending loss; finally, these lasers can be easily scaled down to a centimeter-level [6,7].

In terms of the material option, a medium with a high nonlinear coefficient, a broad transmission window, and a suitable dispersion profile that can produce rich nonlinear effects over relatively short transmission distances is essential [1–3]. High nonlinearity and a broad transmission window are beneficial to generate SC in a wide spectral region,



Citation: Chen, P.; Long, Z.; Cheng, Q.; Song, M.; Wang, W.; Liu, R.; Zhang, Z.; Xia, K.; Yang, Z.; Qian, L.; et al. On-Chip Supercontinuum Generation Pumped by Short Wavelength Fiber Lasers. *Photonics* **2024**, *11*, 440. <https://doi.org/10.3390/photonics11050440>

Received: 7 April 2024
Revised: 19 April 2024
Accepted: 1 May 2024
Published: 9 May 2024



Copyright: © 2024 by the authors. Licensee MDPI, Basel, Switzerland. This article is an open access article distributed under the terms and conditions of the Creative Commons Attribution (CC BY) license (<https://creativecommons.org/licenses/by/4.0/>).

while the suitable dispersion profile can shift the zero-dispersion wavelength (ZDW) to a desired wavelength that can match the suitable pump source available. The ZDW is determined by the material refractive index and the waveguide structural parameters, and the material with a larger refractive index usually has a larger zero dispersive waveguide. For example, chalcogenide glasses with values of the refractive index from 2 to 4 have zero dispersion wavelengths from 3 to 6 μm depending on the structural parameters, while the zero dispersive wavelength in the oxide materials with a refractive index around or below two is from 1 to 2 μm , which can easily be pumped using compact short pulse sources [1–3].

On the other hand, the laser damage threshold is also important since pump lasers with higher power may burn the materials. This is especially important for the waveguide pumped by the laser with a short wavelength laser since such a pump source usually has a high power compared with the mid-infrared fs laser. The advantage of the material with a high laser damage threshold is clear, e.g., the high power and broad expansion of the SC output can be expected from such a waveguide.

Over the past few years, a number of the results on SC generation have been reported in fiber and waveguide. In terms of the width of the SC spectrum, for example, the 2–16 μm SC spectrum has been reported in GeAsTeSe fiber pumped by OPO lasers, and a maximum SC power of several hundred mW has been reported in Refs. [5,8]. However, for these broad SC generations, the pump light is injected into the waveguide or fiber via free-space optical coupling, and the whole optical system is fragile and uncompact. One method is to integrate a waveguide or fiber with a fiber laser via a tapered fiber, forming a compact optical system for practical applications. Therefore, the combination of fiber-based ultra-short-pulsed lasers and waveguides is highly promising for compact, on-chip SC generation. In this review, we focus on such a topic, e.g., pump sources that are limited in the pulse fiber lasers with short wavelengths. A number of materials like SiN and SiO₂, Al₂O₃/AlN, TeO₂, Ta₂O₃, TiO₂, chalcogenides, and LiNbO₃ have been used for SC generation; we will review their optical properties, as well as the SC spectra in the waveguides with different structural parameters and pump sources, respectively. Finally, we point out the existing challenges in the development of a practical SC source in the future.

2. Si and SiN

Silicon-based materials are probably widely used photonic materials due to their excellent optical properties like high transparency in visible and infrared and low optical loss [9]. Si, SiN, and SiO₂ have a refractive index of 3.48, 2.0, and 1.45 at 1.55 μm [10,11], respectively; therefore, SiO₂ is primarily used as the cladding component in conjunction with SiN and Si, forming various special structures.

Alizadeh et al. prepared a waveguide with a silicon core embedded in a thick SiO₂ layer. The light was well confined in the silicon waveguide thanks to the larger contrast of the refractive index between SiO₂ and silicon, as well as the thick cladding layer, avoiding any possible leakage of the light. A supercontinuum spanning from 1100 to 4000 nm was observed while the waveguide was pumped by a 1.89 μm laser with a peak power of 800 W and a pulse duration of 50 fs [12].

Marco et al. fabricated a waveguide with a similar structure, but silicon nitride replaced the core of the waveguide. The waveguide is excited by a 1.56 μm fiber laser emitting pulses lasting 120 fs at a repetition rate of 40 MHz. The pulses are directed into the Si₃N₄ waveguide sample through two half-wave plates, a polarizing beam splitter, and an aspherical lens. A lensed fiber and an off-axis parabolic mirror are used to collect and collimate the generated SC. A curved mirror focuses the beam via a removable mirror into two different optical spectrum analyzers. The subsequent SC spectrum measurements in this paper generally follow this method. The resulting SC spectrum ranges from around 526 nm to at least 2.6 μm [13].

Neetesh et al. demonstrated a wavelength-doubled silicon waveguide spanning the coherent supercontinuum spectrum from the near-shortwave infrared region. When injecting a light with a wavelength of 1550 nm, a pulse width of 100 fs, and a repetition

rate of 200 MHz into highly nonlinear optical fibers, these pulses underwent Raman shift, resulting in pulses with a duration of 450 fs and a wavelength of 1.9 μm [14]. The team used such a laser to pump two waveguides with different core widths, in which the zero-dispersion wavelengths varied from 1.67 μm to 1.1 μm . The supercontinuum broadening for both waveguides was approximately 1.124 μm to 2.4 μm .

Bao et al. proposed that lower waveguide dispersion can be obtained at longer wavelengths from horizontal slot waveguides with much smaller slot thickness [15]. They, therefore, designed two schemes for horizontal double-slot silicon waveguide structures. One option was to use two slots at the bottom of the waveguide, resulting in a supercontinuum broadening from 1464 nm to 2266 nm pumped by a laser with a peak power of 15 W, a center wavelength of 1.7 μm , and a pulse width of 50 fs. Another option was to place two slots on the sides, leading to supercontinuum broadening from 1498 nm to 2376 nm under the same pumping conditions.

Ryosuke et al. utilized a novel micro-transfer printing technique to fabricate a Si-SiO₂-Si horizontal slot waveguide (a silicon-based slot waveguide) [16]. A mode-locked erbium-doped fiber laser with a central wavelength of 1.56 μm , a pulse width of 65 fs, and a repetition rate of 100 MHz was used as the pump source. The dependence of the SC spectrum on the input pulse energy up to 10 pJ is shown in Figure 1a. The broadening of the SC spectrum was mainly due to the initial SPM, and the pulse energy was transferred to spectral components at a wavelength of around 2 μm by the dispersive wave, which was in agreement with the simulation result at the interaction length of 2 mm shown in Figure 1b. The maximal SC bandwidth at 30 dB was from 1.35 μm to 2.05 μm at the coupled pulse energy of 10 pJ. They also found that a further increase in the pump power did not contribute to the broadening of the SC spectrum due to the two-photon absorption of Si.

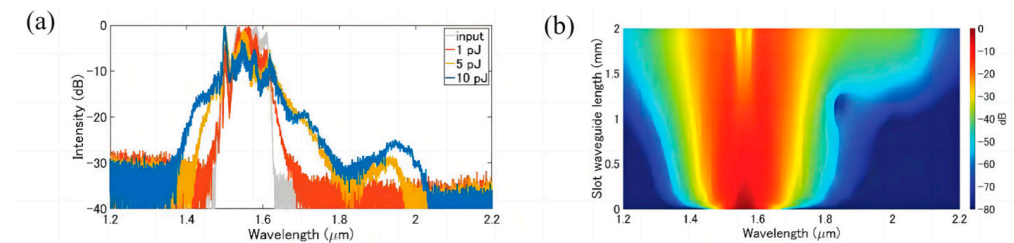


Figure 1. Dependences of SC spectra on (a) input pulse energy (experiment), and (b) waveguide length at a pump energy of 10 pJ (simulation) [16]. Reprinted with permission from [16].

Ahmad et al. simulated the generation of a mid-infrared supercontinuum (SC) in an air-clad silicon nitride (Si₃N₄) waveguide, employing a laser with a pump wavelength of 1.55 μm , an ultra-short pulse duration of 50 fs, and a peak power of 5 kW. The SC spectrum covering a range from 0.8 μm to over 6.5 μm can be achieved in the waveguide with a height of 0.8 μm and a width of 3 μm , and such an SC spectrum can be further broadened at its long wavelength side via increasing the height of the waveguide to 0.9 μm [17].

Guo et al. observed an SC spectrum covering more than two octaves from visible light (0.56 μm) to mid-infrared (3.6 μm) [18] in a 1.7 μm wide SiN waveguide. The pump source used was a compact mode-locked, erbium fiber-based femtosecond laser capable of emitting a pulse sequence with a repetition frequency of approximately 100 MHz. The pulse duration was less than 90 fs, the average power exceeded 110 mW, and the center wavelength was 1550 nm.

David et al. utilized SiN waveguides with different widths pumped by a 100 MHz repetition rate and 1550 nm fiber laser to generate supercontinuum spectra. The SC spectrum in Figure 2 is shown as a function of the waveguide width. This spectrum spans from approximately 500 nm to over 3 μm , covering a bandwidth of two-octave ranges. The third harmonic generation (THG) and dispersive wave (DW) also appear at the short wavelength region [19].

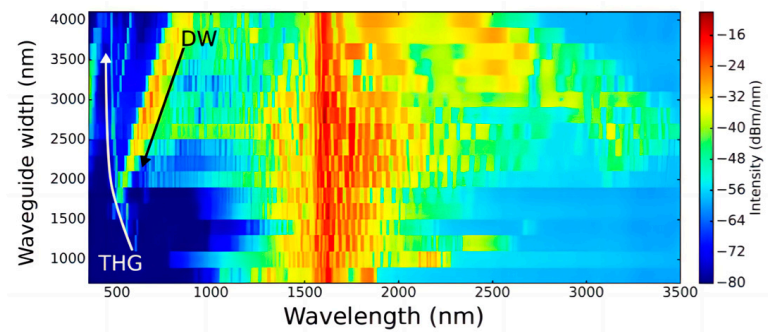


Figure 2. Supercontinuum spectra from SiN waveguides of different waveguide widths pumped with a 100 MHz repetition rate and 1550 nm fiber-laser [19]. Reprinted with permission from [19].

Karim et al. reported a numerical study on the generation of supercontinuum spectra in a novel 5 mm air-clad SiN-suspended core channel waveguide. The proposed waveguide was pumped by a laser with a wavelength of 1.55 μm , a power of 20 kW, and a pulse width of 50 fs. The observed supercontinuum spectrum covered a range from 0.8 μm to 6 μm [20].

Dmitry achieved a supercontinuum spectrum extending from 1.2 to 3.7 μm , covering more than 1.5-octave ranges, by utilizing a 2.35 μm sub-40 fs pulse generated from a 75 MHz Kerr lens mode-locked Cr:ZnS laser in a silicon nitride waveguide [21].

Zhang et al. introduced a novel silicon waveguide with a horizontal silica slot between two silicon layers. This waveguide exhibited four zero-dispersion wavelengths for the first time, with flat dispersion over a bandwidth of 670 nm, and a supercontinuum broadening from 1217 nm to 2451 nm was achieved in the waveguide pumped by a laser with a central wavelength of 1810 nm, a full-width at half-maximum of 120 fs, and a peak power of 62 W [22].

Kuyken et al. demonstrated the generation of a supercontinuum in a 2 cm long silicon wire pumped by a coherent Mira-OPO at a central wavelength of 2120 nm with a pulse width of 2 ps (full-width at half-maximum) and a repetition rate of 76 MHz in the anomalous dispersion regime [23]. Although the pump source was not fiber laser, we still included these results in the paper since the laser wavelength was short. The supercontinuum extended from 1535 nm to 2525 nm, with a coupled peak power of 12.7 W. They also pumped the waveguide with a comb seed source consisting of a home-built mid-infrared OPO with a repetition rate of 100 MHz, synchronously pumped by a mode-locked femtosecond titanium–sapphire laser. The OPO had a center wavelength of 2290 nm, close to the zero-dispersion wavelength of the silicon waveguide at 2180 nm. With a pulse duration of 70 fs and an average power of 35 mW, they simulated the spectral content of the optical pulse along the length of the silicon photonic wire waveguide, as shown in Figure 3a, and ultimately achieved supercontinuum broadening from 1540 nm to 3200 nm [24]. They also measured the SC spectra, which were generally in agreement with the simulated spectral broadening, and the coherence of the pulses was also simulated, as shown in Figure 3b.

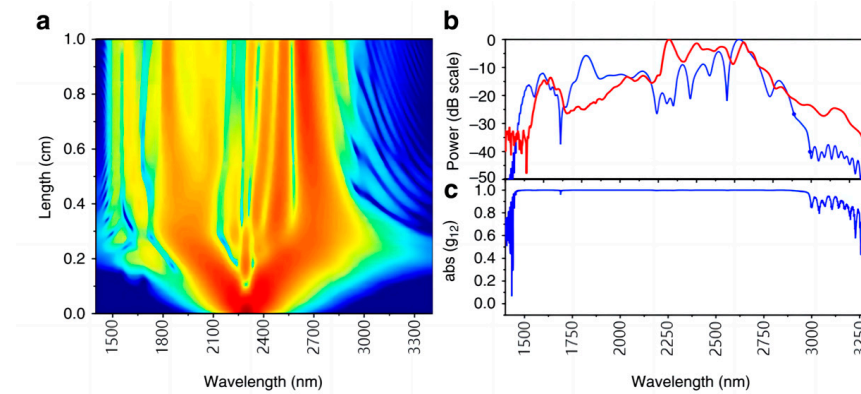


Figure 3. The simulated spectral broadening and coherence of the pulses. (a) Evolution of the spectral content of the optical pulse along the length of the silicon photonic wire waveguide. (b) Simulated spectra after 1 cm of propagation in the waveguide (blue) and the measured supercontinuum (red). (c) Simulated coherence as a function of the wavelength [24]. Reprinted with permission from [24].

3. Al₂O₃ and AlN

Sapphire (Al₂O₃) is a good optical material since it has a broad transmission region of up to 8 μm, a relatively high refractive index of ~1.8, a good nonlinear refractive index value of $n_2 \approx 2.8 \times 10^{-20} \text{ m}^2/\text{W}$, and a high damage threshold (up to 1.3 kJ/cm²) [25].

In the case of sapphire pumped by a short laser wavelength, Kim et al. [25] demonstrated that the broadband SC spectrum (up to 3.2 μm) can be achieved by launching ultra-short femtosecond laser pulses into single crystal sapphire fiber with a dimension of 115 μm in diameter and 5 cm in length, where the 2 μm pumping source is created using an optical parametric amplifier (OPA) seeded by a 784 nm femtosecond laser.

Li et al. inscribed a waveguide from the sapphire crystal using a femtosecond laser [26] and investigated the SC generation from waveguides. Two groups of waveguides with radii of 36 μm and 24 μm (hereafter referred to as WG1 and WGII) were fabricated, respectively. The spectral changes in waveguides and bulk sapphire with a length of 5 mm were examined at an input pulse energy of 7.3 μJ. The pump source had a central wavelength of 1030 nm, a pulse duration of 400 fs, and a repetition rate of 300 kHz, respectively. On the short wavelength side, a relatively steady cut-off wavelength of ~450 nm was found, as shown on the left part of Figure 4, but the WG1 waveguide exhibits much better SC spectra in terms of width and flatness. In the right part of Figure 4, the pump lasers have greater expansion up to 1100 nm, while the image in the inset is their respective far-field image from SC emission. This gives clear evidence that the well-structured waveguide is beneficial to the generation of a broad and flattened SC spectrum.

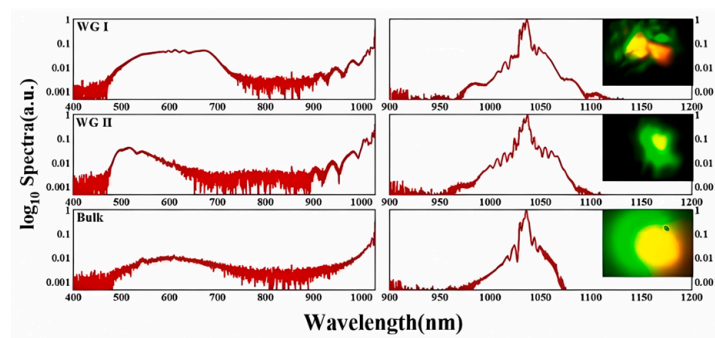


Figure 4. Experimental supercontinuum spectra generated in different forms of sapphire media (i.e., the waveguide of different dimensions and sapphire bulk) under 7.3 μJ input pulse energies. Reprinted with permission from [26].

On the other hand, aluminum nitride (AlN) thin films used in photonics devices are usually polycrystalline or single crystalline and, thus, exhibit both strong $\chi^{(2)}$ and $\chi^{(3)}$. Although polycrystalline waveguides sometimes have a relatively high optical loss, thin-film AlN has been demonstrated to be a versatile platform for nanophotonics, providing unique features like phase-matched second harmonic generation that cannot be observed in the glassy waveguides [27].

Hickstein et al. prepared a fully SiO₂-clad AlN polycrystalline waveguide with a thickness (height) of 800 nm, a width of 3200 nm, and a length of 10 mm. By coupling into the waveguide with 1560 nm light and a power of approximately 80 mW, a pulse width of approximately 80 fs, and a repetition rate of 100 MHz, SC spectra can be excited with a maximal width from the visible region (approximately 500 nm) to the mid-infrared (about 4000 nm), as shown as the red curve in Figure 5, where the experimental results are roughly in agreement with the blue curve of the simulation [27].

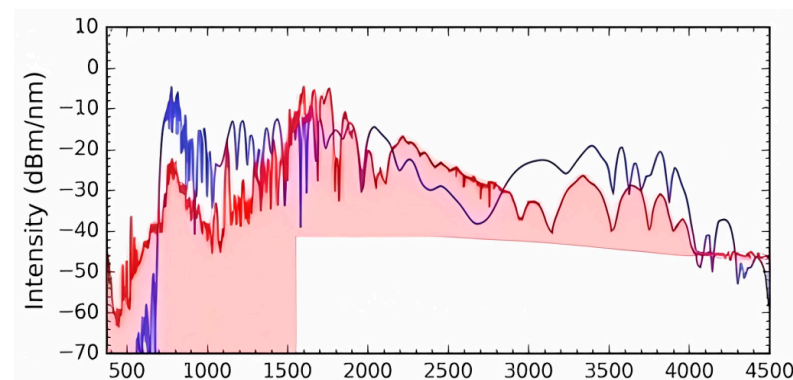


Figure 5. Supercontinuum generation from the lowest-order quasi-transverse-electric (TE₀₀) mode (the red) and the theoretical optical spectrum from the waveguide (the blue). The bottom of the shaded region indicates the noise floor of the OSA. Reprinted with permission from [27].

Lu et al. reported that a single-crystalline AlN film with a thickness of 1 μm was grown on c-plane sapphire by metal-organic chemical vapor deposition, and then oxide-clad AlN waveguides with widths from 0.8 to 3.0 μm were fabricated. The total waveguide length was 8 mm, and each waveguide was tapered to a width of 4 μm at the end facets. SC spectra of the nanophotonic AlN waveguides were characterized by 200 fs wide pulses and a pump wavelength of 1560 nm from a TOPTICA FemtoFiber proNIR with a repetition rate of 80 MHz. They demonstrated a broad SC spanning from UV to MIR wavelengths in dispersion-engineered single crystalline AlN waveguides [28]. Figure 6 shows the supercontinuum spectrum from 400 nm to 4200 nm recorded from a 2.6 $\mu\text{m} \times 1.0 \mu\text{m}$ waveguide; the average power coupled into the waveguide was estimated to be 56 mW, which corresponds to an on-chip pulse energy of ~ 700 pJ. Such a large expansion of the SC into a longer wavelength is mostly due to the high quality of the single crystalline AlN, where the OH absorption is maximally suppressed. The SC spectrum is also highly coherent and in good agreement with the simulation, as shown in Figure 6.

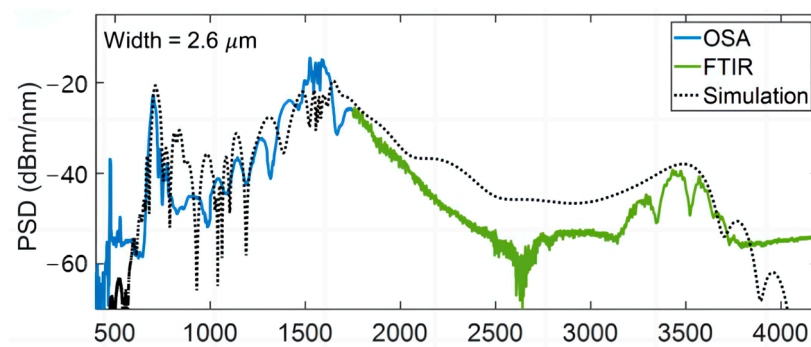


Figure 6. Experimental (solid line) and simulated (dotted line) power spectral density (PSD) from a 2.6 μm wide AlN waveguide with the TE pump. Reprinted with permission from [28].

4. TeO_2

Oxide tellurium (TeO_2) is an ideal candidate material with desirable material properties, such as a high refractive index of 2.1 at 1550 nm and a nonlinear Kerr coefficient that is 30–50 times higher than that of silica [29–32].

Neetesh [33] et al. deposited a tellurium dioxide (TeO_2) layer with a thickness of 370 nm using radio-frequency reactive sputtering on a SiN waveguide with a thickness of 200 nm (T), a width of 1200 nm (W), and a length of 7 mm. The waveguide loss was approximately 0.5 dB/cm [34]. For SC generation, an optical parametric oscillator generating pulses at 1550 nm with a pulse width of 200 fs and a repetition frequency of 80 MHz was used as a pump source. The estimated peak power coupled into the waveguide was 600 W. The output was collected through a multimode fluoride fiber connected to a spectral analyzer. The supercontinuum (SC) spectrum from 1300 nm to 1900 nm generated by the optical parametric oscillator is depicted in Figure 7.

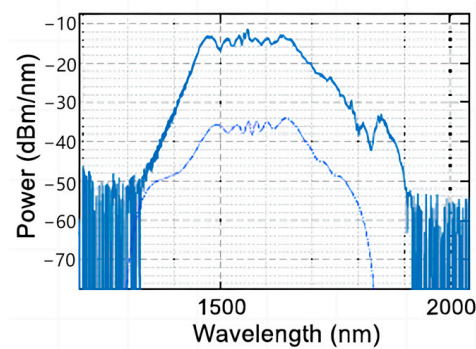


Figure 7. Experimental supercontinuum (solid) and the simulated spectrum (dashed) where the dashed curve is shifted down for clarity. Reprinted with permission from [33].

Hamidu [35] et al. reported SC generation from a highly nonlinear tellurium dioxide (TeO_2) overlapping on a silicon nitride (Si_3N_4) ridge waveguide with a thickness of 400 nm and a width of 1600 nm. The Si_3N_4 chip was fabricated at the Lionix foundry using standard Si_3N_4 LPCVD (Low-Pressure Chemical Vapor Deposition). The TeO_2 layer was deposited using reactive radio-frequency magnetron sputtering at room temperature. In the SC experiment, a mode-locked fiber laser with a center wavelength of 1565 nm, a pulse width of 100 fs, a repetition rate of 200 MHz, and an average power of 76 mW was used to pump a 6.7 cm long serpentine-shaped waveguide. The experimental SC spectra with different levels of pump power are shown in Figure 8a and are in agreement with the simulated results in the corresponding pump power shown in Figure 8b.

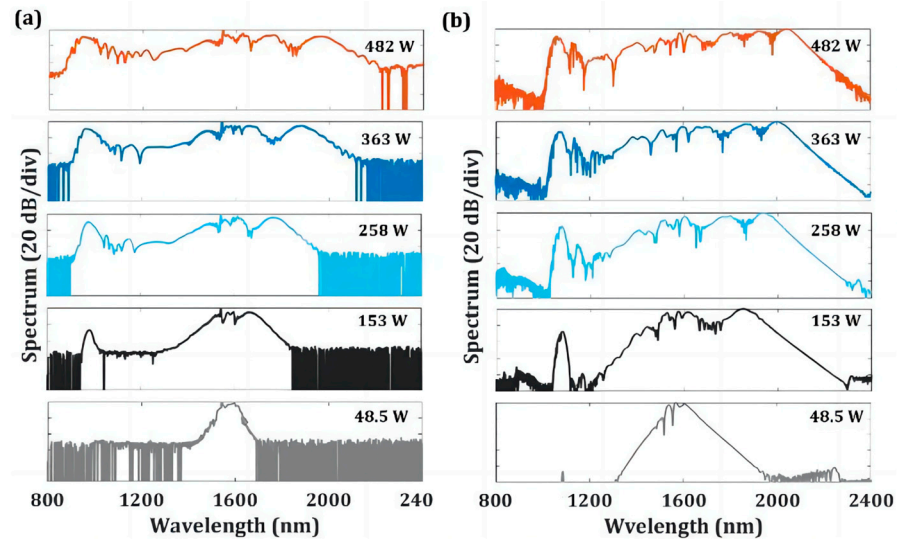


Figure 8. (a) The experimental and (b) simulated SC spectra at different pump powers. Reprinted with permission from [35].

5. Ta₂O₅

Ta₂O₅ has a high refractive index (>2.1), high nonlinear coefficient (n_2 : $\sim 10^{-14}$ cm²/W), wide bandgap (>4.2 eV), low optical loss, and low thermal optical characteristic ($dn/dT < 10^{-6}$ /K), and a high laser damage threshold (few J/cm²), making it useful for optical devices, especially in relation to high-power operation [36–44].

Lee’s group from Taiwan conducted a detailed simulation of the waveguide design and dispersive tuning. In an air-cladding waveguide with a length of 5 mm and a loss of 1.5 dB/cm, they demonstrated an SC spectrum from 585 to 1697 nm pumped by the 1056 nm laser with a pulse duration of 100 fs and a repetition rate of 80 MHz [36]. As shown in Figure 9a, most of the spectral broadening was formed after the propagation of approximately 3.7 mm because high order dispersion and the accumulated nonlinear phase broke up the pulse in the temporal domain known as soliton fission; it offers rapid intensity variation, and larger nonlinear phase modulation is induced to produce new frequency components. The typical SC spectrum in Figure 9b pumped at 396 W power is in excellent agreement with the simulation.

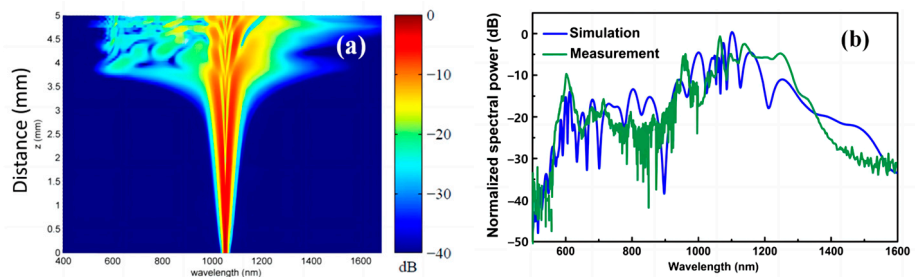


Figure 9. The evolution of SC spectral intensity as a function of propagation distance (a), and the comparison of the simulated and measured spectra (b). Reprinted with permission from [36].

They further investigated the high-order mode SC generation in the Ta₂O₅ waveguide and demonstrated an SC spectrum spanning from 842 to 1462 nm (at –30 dB), which corresponds to 0.83 octaves using the TM10 waveguide mode. They also discussed the possibility of using the broadband higher-order modes emitted from the Ta₂O₅ waveguide for trapping nanoparticles. This is an interesting case to develop a new application of the SC source [37].

Recently, several reports have demonstrated the further expansion of SC from 700 nm to 2400 nm in the waveguide pumped by a 1560 nm laser [42,43], as shown in Figure 10.

The SC spectrum appears to become broad with a decreasing waveguide width, probably due to its improved single-mode propagation feature. Moreover, the low optical loss of around 0.1 dB/cm in the waveguides is beneficial to generate wide SC spectra from 700 nm to 2400 nm in Refs. [42,43].

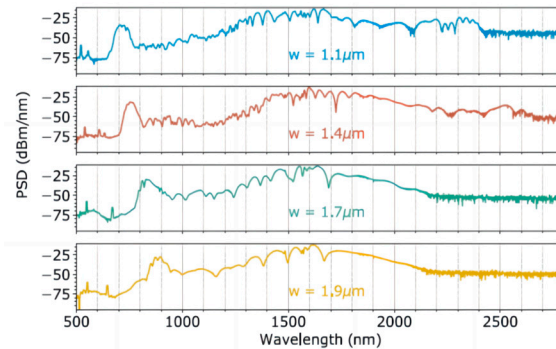


Figure 10. Experimental SC PSD from four different waveguide widths at 80 fs pulse duration and 0.9 nJ/pulse. Reprinted with permission from [42].

6. TiO₂

TiO₂ has a nonlinear index ($\sim 0.2 \times 10^{-18}$ m²/W) and a linear refractive index of 2.4, and these properties could potentially lead to the stronger confinement of light and higher effective nonlinearities in the waveguide. However, this material is largely unexplored in the field of nonlinear photonics. Moreover, negligible two-photon absorption in TiO₂ makes it promising to integrate with Si-based materials.

Zhang et al. simulated a compact dual-core waveguide consisting of SiN and TiO₂ with a large enough index contrast for dispersion engineering and obtained an octave-spanning supercontinuum generation from 1160 to 2385 nm at a greatly reduced propagation distance of 165 μm [45]. Shen et al. further designed a strip TiO₂ waveguide with three zero-dispersion wavelengths and simulated a SC covering a wavelength range from 1.71 to 9.90 μm (more than 2.5 octaves) while being pumped by a 3.1 μm laser [46]. Ryu et al. designed dispersion and modal confinement in a TiO₂ slot waveguide and achieved one or two-octave broadband SC spectra in two waveguides with different structures [47].

Experimentally, Hammani et al. demonstrated the generation of an octave-spanning supercontinuum from 1 to 2.4 μm in a 2.2 cm long TiO₂ waveguide with two zero dispersion wavelengths. The resulting on-chip supercontinuum reached the visible wavelength range as well as the mid-infrared region using a femtosecond fiber laser pump at 1.64 μm [48]. Evans et al. observed spectral broadening in single-mode TiO₂ waveguides pumped by 1565 and 794 nm femtosecond pulses. However, the expansion of SC spectra was poor. Nevertheless, they concluded no two-photon absorption in the waveguides [49].

7. Chalcogenide

Chalcogenide materials have broad transmission regions, a high linear and nonlinear refractive index, and low two-photon absorption and are highly suitable not only for nonlinear applications but also for compact active and passive devices in the mid-infrared region. Chalcogenides are also featured with broad glass-forming regions, and thus, their physical properties, like the linear and nonlinear refractive index, can be tuned into a wide compositional range. Many chalcogenide glasses with different compositions have been used for waveguide fabrication [50]. Since chalcogenide glasses have a relatively high refractive index, their ZWD is usually located at 3–7 μm in the waveguides prepared by UV lithography; therefore, mid-infrared OPO lasers are mostly used as pump sources [2]. For example, SC spectra from 2–5 μm to 2–10 μm have been reported in As₂S₃ [51] and GeAsSe [5] waveguides, respectively. In contrast, the spectra pumped by short-wavelength fiber laser remain relatively less investigated.

In As_2S_3 , Lamont et al. and Hwang et al. [52,53] demonstrated SC generation in the As_2S_3 chalcogenide waveguide pumped by $1.55 \mu m$ fs pulsed lasers. The typical SC spectral bandwidth was from 1.1 to around $2.2 \mu m$. Recently, we developed a dual-femtosecond soliton pulse laser to pump the As_2S_3 waveguide with different widths and achieved a span of SC from 1500 to 2400 nm in the waveguide with a width of $1 \mu m$ and a height of 870 nm. The results are shown in Figure 11, where the experimental spectrum is generally in agreement with the simulation.

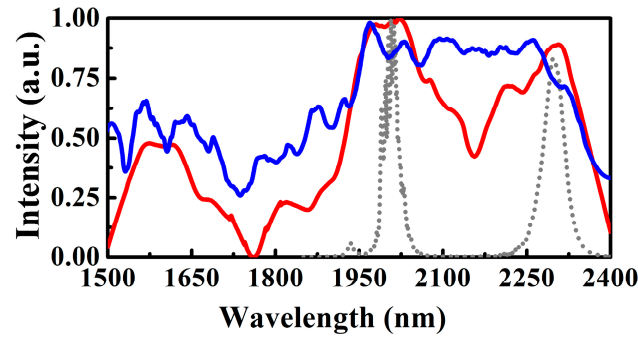


Figure 11. SC in As_2S_3 waveguide pumped by the dual-soliton pulsed laser; the grey dot lines correspond to the pump laser, and the red is the experimental result while the blue is the simulation.

$Ge_{11.5}As_{24}Se_{64.5}$ glass was reported to be a stable composition against any external energy input, like thermal annealing, light illumination, γ -ray, and X-ray irradiation [54,55], and thus, it is widely used for the chalcogenide waveguide. Gai et al. and Shang et al. [56–58] reported SC generation in $Ge_{11.5}As_{24}Se_{64.5}$ waveguides pumped by the $1.55 \mu m$ laser. With increasing pump power, the SC spectra broaden from $1 \mu m$ to $2 \mu m$, as shown in Figure 12.

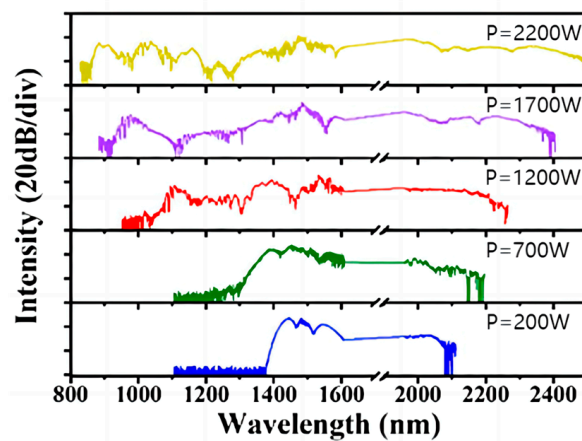


Figure 12. Experimental SC evolution with increasing pump powers. Reprinted with permission from [58].

GeSbS and GeSbSe were also used to prepare the waveguides since a heavy element, Sb, in the glass can improve the optical nonlinearity [59–64]. Choi et al. succeeded in fabricating the GeSbS waveguide with a length of 15 mm and obtained SC spectra from 1.28 to $2.12 \mu m$, as depicted in Figure 13, when the waveguide was pumped by $1.55 \mu m$ laser with peak power and a pulse width of 340 W and 500 fs, respectively.

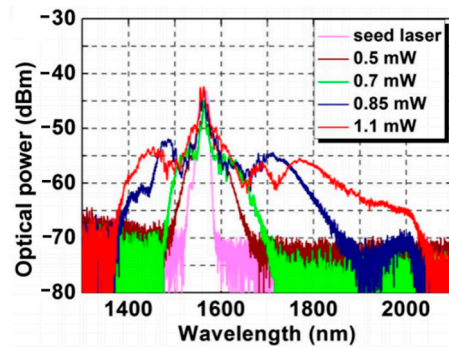


Figure 13. SC spectra from a GeSbSe waveguide at different pump power levels. The power quoted here represents the average optical power coupled into the waveguide. Reprinted with permission from [63].

8. LiNbO₃

Lithium niobate (LiNbO₃, LN) has excellent optical properties, like a wide transparent window (0.35~5 μm), large band gap (3.8 eV), larger refractive index (approximately 2.2 at 1550 nm) and high nonlinear coefficient. These properties make it widely used in high-speed modulators [65], single-photon sources, mid-infrared frequency comb [66], optical parametric oscillators [67], and SC light emitters.

In terms of SC generation, Yu et al. [68] succeeded in fabricating the LN waveguide with a length of 0.5 cm and obtained SC spanning from 0.4 to 2.4 μm using a laser with peak power, wavelength, and pulse width of 1.17 kW, 1.506 μm and 160 fs, respectively. Guo et al. [69] used a 1550 nm pulse with 30 nJ of pulse energy and 150 fs of pulse duration to pump unpoled LN ridge waveguides to obtain an SC spectrum from 1.3 to 3.2 μm .

Through dispersion engineering, the wider and flatter dispersion curve can be effectively tuned in the waveguide. Jing et al. [70] designed the dual-coupled waveguide on a 1.2 mm x-cut LNOI, where four zero-dispersion wavelengths were achieved. When the waveguide was pumped by a 1550 nm laser with a pulse duration of 75 fs and a repetition rate of 100 MHz, the supercontinuum spectrum was generated from 1920 to 3550 nm (-20 dB level, near octave-spanning) at a peak power of 4.5 kW (pulse energy is 190 pJ). Lu et al. [71] designed and prepared a waveguide with air cladding and achieved a SC spectrum from 700 to 2200 nm at -30 dB in a 10 mm long waveguide, as shown in the main panel of Figure 14, where the experimental spectrum is in good agreement with the simulation. Strong third-order harmonic dispersion waves can also be observed, as shown in the inset of Figure 14 (green and yellow lines).

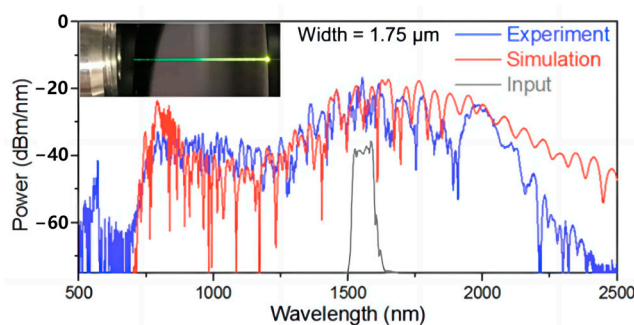


Figure 14. Experimental and simulated SC spectra; the inset is an image of the waveguide where the green and yellow colors are from the third-order dispersive waves of the pump laser. Reprinted with permission from [71].

Wu et al. [72] designed a novel nanophotonic multi-segmented nonlinear thin film LN waveguide with an aim to extend SC into the ultraviolet short-wave region. When the waveguide with a width of 1.8 μm was pumped by a 550 nm laser with a pulse duration of

130 fs, an SC spectrum range from 330 to 2400 nm could be generated. The inset clearly shows that the pump light can be converted into yellow, green, blue, and violet along the light propagation direction via various nonlinear processes. Yu et al. [73] even achieved a much broader SC spectrum, approximately from 350 to 4100 nm, considering the second- and third-order nonlinear interactions in the waveguide.

LNO waveguides were also pumped by the laser with a wavelength of ~2.0 μm. In 5 mm length nanophotonic periodically poled lithium niobate waveguides, Marc et al. [74] achieved an SC spectrum from 400 to 2400 nm. C. R. Phillips [75] demonstrated an SC spectrum from 1350 to 2800 nm in the waveguide pumped by a 1930 nm laser with a pulse duration of 97 fs and a repetition rate of 72 MHz.

For the pump lasers at even shorter wavelengths of less than 1.5 μm, Marc et al. [76] used 950 nm to pump 14 mm non-centrosymmetric lithium niobate-on-insulator ridge waveguides to extend SC light to near-ultraviolet (NUV) light. When the laser with a pulse width of 50 fs and an energy of 67 pJ was injected into the waveguide (equivalent peak power of 266 W), the SC spectra range from approximately 710 to 1230 nm was achieved, as shown in Figure 15. Guo et al. [77] also investigated soliton-induced SC experimentally and obtained an SC spectrum from 900 to 2200 nm while pumping using a 1250 nm laser with a pulse duration of 50 fs and a peak power of 20 kW.

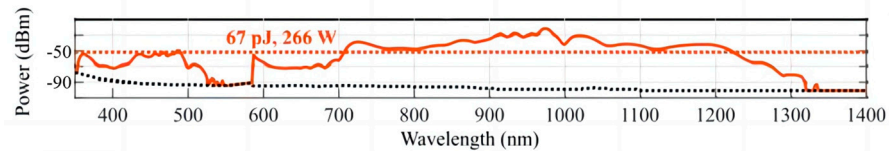


Figure 15. SC spectra in LNO waveguide pumped by 950 nm laser. The orange dashed line represents the 30 db bandwidth of each generated signal, and the black dashed line indicates the noise threshold of the spectrum analyzer [76]. Reprinted with permission from [76].

9. Opportunities and Challenging

Over the past decade, there has been considerable progress in developing integrated SC sources pumped by short-wavelength lasers for various applications. Table 1 lists the physical properties and SC parameters of the typical materials that are reviewed in the paper. Some materials are probably missed for SC generation pumped by short wavelength lasers. For example, waveguides like Ge/GeSi and GaAs/AlGaAs requiring pump sources with long wavelengths are excluded in the paper. The waveguides based on tellurite and phosphate glasses are not contained as well due to their complicated compositions. Nevertheless, the results in the present paper still represent the most achievements in this area until now.

Table 1. Physical properties and SC parameters of the materials that are reviewed in this paper.

Material	Refractive Index@1.5 μm	Third-Order Nonlinearity (cm ² /W)	Transmission Range (μm)	Pump Wavelength (μm)	Maximum Range of SC Spectrum (μm)	Ref.
Al ₂ O ₃	1.75	3 × 10 ⁻¹⁶	0.18–4.5	1.03	0.45–1.1	[26]
AlN	2.2	2.3 × 10 ⁻¹⁵	0.2–5.5	1.56	0.4–4.2	[28]
Ta ₂ O ₅	2.0	~10 ⁻¹⁴	0.5–8	1.55	0.5–2.5	[36–44]
TeO ₂	2.1	1.4 × 10 ⁻¹⁴	0.33–5.0	1.565	0.9–2.2	[35]
TiO ₂	2.4	9.4 × 10 ⁻¹⁵	1–9	1.64	1–2.4	[48]
Chalcogenide	2.2–3	5–15 × 10 ⁻¹⁴	0.5–15	1.55	1.28–2.12	[62]
LiNbO ₃	2.21	1.8 × 10 ⁻¹⁵	0.35–5	1.55	0.35–4.1	[73]
SiN	2.0	2.4 × 10 ⁻¹⁵	0.35–7	1.55	0.56–3.6	[18]
Si	3.48	6.0 × 10 ⁻¹⁴	1.1–9	1.55	1.124–2.4	[14]

We can see from Table 1 that most of the materials have a nonlinear refractive index at around 10⁻¹⁴–10⁻¹⁶ cm²/W, and the spanning of SC is always limited below 2.5 μm.

It appears that the difference in the nonlinear refractive index has a negligible effect on the broadening of the SC spectrum. This is due to the fact that these materials (excluding chalcogenides) usually have a larger laser damage threshold, and thus, nonlinear broadening can be achieved via a larger pump power from fiber-based short-wavelength lasers. Therefore, the limit of SC spanning below 2.5 μm could be for other reasons. For example, the coupling of the light into and out of the waveguide is mostly based on tapered silica fiber; therefore, the expansion of the SC spectrum in the long wavelength is limited by the absorption of silica beyond 3 μm . The use of fluorite [18] and chalcogenide fibers can certainly deliver the signal of the long wavelength into the detector, but this usually leads to issues like the matching of the mode field, and thus, the optical internal connection has been an unsolved problem in the development of an integrated SC source pumped by short wavelength fiber lasers.

Another possible reason that can account for the limitation of the SC broadening beyond 3 μm is the strong OH absorption at 2.92 μm . When such an absorption in the fiber can be reduced via careful material purification, it is challenging to be suppressed in the waveguide. Although the absorption from the defects can be maximumly reduced in the deposition target, OH-related defects can be introduced again when the target is decomposed and re-condensed into the films in the vacuum since the residual OH- and H- species in the vacuum can react with decomposed ions and clusters in the chamber. The intensity of the absorption at 2.92 μm is determined by the number of OH-related defects, and the extension of the SC spectra at a longer wavelength can be limited by such an absorption. Therefore, the suppression of such absorption is key to realizing the broadening of the SC spectrum beyond 3 μm , but this has not been solved or has never been emphasized in the literature.

Exceptions can be found in Table 1, where both AlN and LiNbO₃ have an SC beyond 3.0 μm . Since AlN and LiNbO₃ used in the literature [28,73] are bulk single crystals, the content of OH absorption in the materials is significantly suppressed.

On the other hand, the emission wavelength of most of the fiber sources is around 1.0–2.0 μm , and to maximize the width of the SC output, ZDW in the waveguide should be moved to a short wavelength, and this usually leads to the small geometry of the waveguide structure, typically around hundreds of nanometers in width and height. Therefore, traditional UV lithography plus chemical etching cannot be applied to waveguide fabrication. While E-beam lithography is a solution that can produce high-quality waveguides, it is challenging to etch hard oxide materials like Ta₂O₅. Physical etching, like ion milling, is possible, but the processing parameters for individual materials should be further optimized.

Nevertheless, the quality of the waveguide is also important to achieve a broad SC output. The rough surface and sidewall in the waveguide usually lead to large optical loss. To investigate this, Grayson et.al. measured the line roughness of the waveguide and estimated the scattered loss [78]. Considering the intrinsic loss, they claimed the existence of 1.1 dB/cm excess loss in the GeSbSe waveguide but not in the GeSbS waveguide. Such an excess loss was assigned to different surface states in GeSbSe and GeSbS waveguides. In GeSbSe, surface reactions with the surrounding environment result in precipitates of oxides and changes with atomic concentrations, which could significantly affect the properties of the glass, while in GeSbS, the formation of a germanium oxy-sulfide glass at the surface could act as a passivation layer or at least result in a surface that behaves similarly to the original GeSbS chalcogenide. It was also reported that light illumination with different levels of photon energy and power can induce extra optical loss in chalcogenide waveguides [79]. Recently, we proposed and demonstrated an interesting structure in chalcogenide waveguides [80], where a trapezoidal SiO₂ structure was first formed, and then the film was deposited in a direction normal to the wafer surface. In this case, the etchless waveguide exhibited a propagation loss of around a few dB/m, which is one order of magnitude lower than those obtained in the traditional chalcogenide waveguide. This

could be one of the solutions to fabricate a high-quality waveguide. However, this has not been investigated in oxide waveguides.

We also note that one difference in the SC spectra pumped by the mid-infrared OPO laser and short-wavelength fiber laser is the sharp, separated peaks that appear in the short wavelength region, typically in a range from 500 to 800 nm. This usually is ascribed to the dispersive waves. In a recent paper, Wu et al. demonstrated that it is possible to achieve the SC spectrum to UV region in the waveguide assisted by these dispersive waves [72]. However, since the Rayleigh scattering is proportional to the inverse wavelength to the fourth power, this further amplifies the importance of the high-quality waveguide with low optical loss to achieve an SC source down to the UV region. On the other hand, this also could be limited by the transparent cutting-off edge in the materials. Nevertheless, the development of an SC source in the UV region is interesting for various practical applications and is expected to attract more attention from researchers soon.

In summary, there are exciting opportunities to exploit the novel properties of on-chip SC sources pumped by short-wavelength lasers. Recent results are very encouraging, showing that it is possible to obtain low-loss or highly nonlinear waveguide devices tailored for important applications. Exciting developments can be anticipated as further optimization is applied to create new opportunities in optical science.

Author Contributions: Conceptualization, R.W.; methodology, P.X., P.Y. and R.W.; investigation, P.C., Z.L., Q.C., M.S., W.W., R.L., Z.Z., K.X., Z.Y. and L.Q.; writing—original draft preparation, P.C., Z.L., Q.C., M.S., W.W. and R.W.; writing—review and editing, P.X., P.Y., S.B. and R.W.; visualization, P.C. and Z.L.; supervision, X.W., E.S.Y. and R.W.; project administration, R.W.; funding acquisition, E.S.Y. and R.W. All authors have read and agreed to the published version of the manuscript.

Funding: National Key R&D Program of China (2020YFB1805900); 3315 Innovation Team in Ningbo City, Zhejiang Province, China; K.C. Wong Magna Fund in Ningbo University, China; Open Project Program of Wuhan National Laboratory for Optoelectronics NO. 2022WNLOKF001. and the K.C. Wong Magna Fund in Ningbo University. One of the authors (El Sayed Yousef) extends his appreciation to University Higher Education Fund under Research support Program for Central Labs at King Khalid University through the project number CL/PR1/B/3.

Institutional Review Board Statement: Not applicable.

Informed Consent Statement: Not applicable.

Data Availability Statement: Figure 11 presented in the paper are not publicly available but may be obtained from the authors upon reasonable request. Restrictions apply to the availability of other data. Data were obtained for reuse of the figures from the Optica Publishing Group copyright for Figures 2, 6, 9, 10 and 14; from Elsevier for Figures 4 and 12; from Chinese Laser Press for Figures 7 and 13 via prjournal@siom.ac.cn; from personal permission from Dr. Rai Kou via rai.kou-takahashi@aist.go.jp for Figure 1; from Nature Publishing Group (Nature Communication) for Figure 3; from American Physical Society (Physical Review Applied) for Figure 5; from Arxiv for Figure 8; from Amer Inst Physics (APL Photonics) for Figure 15.

Conflicts of Interest: The authors declare no conflicts of interest.

References

1. Dudley, J.M.; Tayloe, J.R. *Supercontinuum Generation in Optical Fibers*; Cambridge University Press: Cambridge, UK, 2010.
2. Yu, Y.; Gai, X.; Wang, T.; Ma, P.; Wang, R.; Yang, Z.; Choi, D.Y.; Madden, S.J.; Luther-Davies, B. Mid-infrared supercontinuum generation in chalcogenides. *Opt. Mater. Express* **2013**, *3*, 1075–1086. [[CrossRef](#)]
3. Fang, Y.; Bao, C.; Li, S.; Wang, Z.; Geng, W.; Wang, Y.; Han, X.; Liang, J.; Zhang, W.; Pan, Z.; et al. Recent Progress of Supercontinuum Generation in Nanophotonic Waveguides. *Laser Photonics Rev.* **2023**, *27*, 2200205. [[CrossRef](#)]
4. Petersen, C.R.; Moller, U.; Kubat, I.; Zhou, B.; Dupont, S.; Ramsay, J.; Benson, T.; Sujecki, S.; Abdel-Moneim, N.; Tang, Z.; et al. Mid-infrared supercontinuum covering the 1.4–13.3 μm molecular fingerprint region using ultra-high NA chalcogenide step-index fibre. *Nat. Photonics* **2014**, *8*, 830–834. [[CrossRef](#)]
5. Yu, Y.; Gai, X.; Ma, P.; Choi, D.Y.; Yang, Z.; Wang, R.; Debbarma, S.; Madden, S.J.; Luther-Davies, B. A stable, broadband, quasi-continuous, mid-infrared supercontinuum generated in a chalcogenide glass waveguide. *Laser Photonics Rev.* **2014**, *8*, 792–798. [[CrossRef](#)]

6. Xia, K.; Yang, Z.; Zhao, P.; Yang, P.; Xu, P.; Xu, L.; Peng, X.; Zhang, W.; Dai, S.; Wang, R.; et al. Supercontinuum generation in As₂S₃ chalcogenide waveguide pumped by all-fiber structured dual-femtosecond solitons. *Opt. Express* **2023**, *31*, 29440–29451. [[CrossRef](#)]
7. Wang, H.; Yang, L.; Yang, Z.; Kang, Z.; Yang, P.; Zhang, W.; Wang, R.; Xu, P. Nanophotonic chalcogenide waveguides for supercontinuum generation pumped at 1550 nm. *Infrared Phys. Technol.* **2024**. [[CrossRef](#)]
8. Zhao, Z.; Wu, B.; Wang, X.; Pan, Z.; Liu, Z.; Zhang, P.; Shen, X.; Nie, Q.; Dai, S.; Wang, R. Mid-infrared supercontinuum covering 2.0–16 μm in a low-loss telluride single-mode fiber. *Laser Photonics Rev.* **2017**, *11*, 1700005. [[CrossRef](#)]
9. Su, Y.; Zhang, Y.; Qiu, C.; Guo, X.; Lu, S. Silicon photonic platform for passive waveguide devices: Materials, fabrication, and applications. *Adv. Mater. Technol.* **2020**, *5*, 1901153. [[CrossRef](#)]
10. Yao, S.; Han, H.; Jiang, S.; Xiang, B. Design, simulation, and analysis of optical microring resonators in lithium tantalate on insulator. *Crystals* **2021**, *11*, 480. [[CrossRef](#)]
11. Kim, D.S.; Yoon, S.G.; Jang, G.E.; Suh, S.J.; Kim, H.; Yoon, D.H. Refractive index properties of SiN thin films and fabrication of SiN optical waveguide. *J. Electroceramics* **2006**, *17*, 315–318. [[CrossRef](#)]
12. Alizadeh, M.R.; Seifouri, M.; Olyae, S. Numerical Investigation and Design of Optical On-Chip Waveguide with Engineered Dispersion for Generation of Supercontinuum-Based Frequency Combs. *Silicon* **2023**, *15*, 7441–7452. [[CrossRef](#)]
13. Porcel, M.A.; Schepers, F.; Epping, J.P.; Hellwig, T.; Hoekman, M.; Heideman, R.G.; Boller, K.J. Two-octave spanning supercontinuum generation in stoichiometric silicon nitride waveguides pumped at telecom wavelengths. *Opt. Express* **2017**, *25*, 1542–1554. [[CrossRef](#)]
14. Singh, N.; Xin, M.; Vermeulen, D.; Shtyrkova, K.; Li, N.; Callahan, P.T.; Magden, E.S.; Ruocco, A. Octave-spanning coherent supercontinuum generation in silicon on insulator from 1.06 μm to beyond 2.4 μm. *Light Sci. Appl.* **2018**, *7*, 17131. [[CrossRef](#)]
15. Bao, C.; Yan, Y.; Zhang, L.; Yue, Y.; Ahmed, N.; Agarwal, A.M.; Kimerling, L.C.; Michel, J.; Willner, A.E. Increased bandwidth with flattened and low dispersion in a horizontal double-slot silicon waveguide. *J. Opt. Soc. Am. B* **2015**, *32*, 26–30. [[CrossRef](#)]
16. Sato, R.; Kou, R.; Yamamoto, N.; Atsumi, Y.; Cong, G.; Murai, T.; Maegami, Y.; Ishizawa, A.; Yamada, K.; Kita, T. Supercontinuum Generation in Si-SiO₂-Si Horizontal Slot Waveguide Fabricated by μ-Transfer Printing. In *Technical Digest Series, Proceedings of the CLEO: Applications and Technology 2023, San Jose, CA, USA, 7–12 May 2023*; paper JTU2A.92; Optica Publishing Group: Washington, DC, USA, 2023. [[CrossRef](#)]
17. Ahmad, H.; Karim, M.R.; Rahman, B.M.A. Dispersion-engineered silicon nitride waveguides for mid-infrared supercontinuum generation covering the wavelength range 0.8–6.5 μm. *Laser Phys.* **2019**, *29*, 025301. [[CrossRef](#)]
18. Guo, H.; Herkommer, C.; Billat, A.; Grassani, D.; Zhang, C.; Pfeiffer, T.J. Mid-infrared frequency comb via coherent dispersive wave generation in silicon nitride nanophotonic waveguides. *Nat. Photonics* **2018**, *12*, 330–335. [[CrossRef](#)]
19. Carlson, D.R.; Hickstein, D.D.; Lind, A.; Droste, S.; Westly, D.; Nader, N.; Coddington, I. Self-referenced frequency combs using high-efficiency silicon-nitride waveguides. *Opt. Lett.* **2017**, *42*, 2314–2317. [[CrossRef](#)] [[PubMed](#)]
20. Karim, M.; Shafiq, T.; Siddique, M.A.; Faisal, M. Suspended core SiN channel waveguide for broadband supercontinuum generation. In *Proceedings of the IEEE International Conference on Telecommunications and Photonics (ICTP), Dhaka, Bangladesh, 22–24 December 2021*; pp. 1–5. [[CrossRef](#)]
21. Martyshkin, D.; Fedorov, V.; Kesterson, T.; Vasilyev, S.; Guo, H.; Liu, J.; Weng, W. Visible-near-middle infrared spanning supercontinuum generation in a silicon nitride (Si₃N₄) waveguide. *Opt. Mater. Express* **2019**, *9*, 2553–2559. [[CrossRef](#)]
22. Zhang, L.; Lin, Q.; Yue, Y.; Yan, Y.; Beausoleil, R.G.; Willner, A.E. Silicon waveguide with four zero-dispersion wavelengths and its application in on-chip octave-spanning supercontinuum generation. *Opt. Express* **2012**, *20*, 1685–1690. [[CrossRef](#)]
23. Kuyken, B.; Liu, X.; Osgood, R.M.; Baets, B.; Roelkens, G. Mid-infrared to telecom-band supercontinuum generation in highly nonlinear silicon-on-insulator wire waveguides. *Opt. Express* **2011**, *19*, 20172–20181. [[CrossRef](#)]
24. Kuyken, B.; Ideguchi, T.; Holzner, S.; Yan, M.; Hansch, T.W.; Campenhout, J.V.; Verheyen, P.; Coen, S.; Leo, F. An octave-spanning mid-infrared frequency comb generated in a silicon nanophotonic wire waveguide. *Nat. Commun.* **2015**, *6*, 6310. [[CrossRef](#)] [[PubMed](#)]
25. Kim, J.H.; Chen, M.K.; Yang, C.E.; Lee, J.; Yin, S.; Ruffin, P.; Edwards, E.; Brantley, C.; Luo, C. Broadband IR supercontinuum generation using single crystal sapphire fibers. *Opt. Express* **2008**, *16*, 4085–4093. [[CrossRef](#)] [[PubMed](#)]
26. Li, Y.; Wu, J.; Zhou, H.; Deng, G.; Zhou, S. Comparison of supercontinuum generation in bulk sapphire and femtosecond-laser-inscribed waveguides. *Opt. Laser Technol.* **2023**, *158*, 108908. [[CrossRef](#)]
27. Hickstein, D.D.; Jung, H.; Carlson, D.R.; Lind, A.; Coddington, I.; Srinivasan, K.; Ycas, G.G.; Cole, D.C.; Kowligy, A.; Fredrick, C.; et al. Ultrabroadband supercontinuum generation and frequency-comb stabilization using on-chip waveguides with both cubic and quadratic nonlinearities. *Phys. Rev. Appl.* **2017**, *8*, 014025. [[CrossRef](#)]
28. Lu, J.; Liu, X.; Bruch, A.W.; Zhang, L.; Wang, J.; Yan, J.; Tang, H.X. Ultraviolet to mid-infrared supercontinuum generation in single-crystalline aluminum nitride waveguides. *Opt. Lett.* **2020**, *45*, 4499–4502. [[CrossRef](#)]
29. Shen, S.; Jha, A.; Liu, X.; Naftaly, M.; Bindra, K.; Henry, J.B.; Ajoy, K.K. Tellurite glasses for broadband amplifiers and integrated optics. *J. Am. Ceram. Soc.* **2002**, *85*, 1391–1395. [[CrossRef](#)]
30. Kim, S.H.; Yoko, T.; Sakka, S. Linear and nonlinear optical properties of TeO₂ glass. *J. Am. Ceram. Soc.* **1993**, *76*, 2486–2490. [[CrossRef](#)]
31. Kim, S.H.; Yoko, T. Nonlinear Optical Properties of TeO₂-Based Glasses: MO_x-TeO₂ (M= Sc, Ti, V, Nb, Mo, Ta, and W) Binary Glasses. *J. Am. Ceram. Soc.* **1995**, *78*, 1061–1065. [[CrossRef](#)]

32. Madden, S.J.; Vu, K.T. Very low loss reactively ion etched Tellurium Dioxide planar rib waveguides for linear and non-linear optics. *Opt. Express* **2009**, *17*, 17645–17651. [[CrossRef](#)]
33. Singh, N.; Mbonde, H.M.; Frankis, H.C.; Erich, I.; Bradley, J.D.B.; Franz, X.K. Nonlinear silicon photonics on CMOS-compatible tellurium oxide. *Photonics Res.* **2020**, *8*, 1904–1909. [[CrossRef](#)]
34. Frankis, H.C.; Kiani, K.M.; Bonneville, D.B.; Zhang, C.; Norris, S.; Mateman, R.; Leinse, A.; Bassim, N.D.; Knights, A.P.; Bradley, J.D.B. Low-loss TeO₂-coated Si₃N₄ waveguides for application in photonic integrated circuits. *Opt. Express* **2019**, *27*, 12529–12540. [[CrossRef](#)]
35. Mbonde, H.M.; Singh, N.; Frare, B.L.S.; Sinobad, M.; Ahmadi, P.T.; Hashemi, B.; Bonneville, D.B.; Mascher, P.; Kaertner, F.X.; Bradley, J.D.B. Octave-spanning supercontinuum generation in a CMOS-compatible thin Si₃N₄ waveguide coated with highly nonlinear TeO₂. *arXiv* **2023**, arXiv:2309.08318. [[CrossRef](#)]
36. Fan, R.; Wu, C.L.; Lin, Y.Y.; Liu, C.Y.; Hwang, P.S.; Liu, C.W.; Qian, J.; Shin, M.H.; Huang, Y.J.; Chiu, Y.J.; et al. Visible to near-infrared octave spanning supercontinuum generation in tantalum pentoxide (Ta₂O₅) air-cladding waveguide. *Opt. Lett.* **2019**, *44*, 1512–1515. [[CrossRef](#)] [[PubMed](#)]
37. Fan, R.; Lin, Y.Y.; Chang, L.; Boes, A.; Bowers, J.; Liu, J.W.; Lin, C.H.; Wang, T.K.; Qiao, J.; Kuo, H.C.; et al. Higher order mode supercontinuum generation in tantalum pentoxide Ta₂O₅ channel waveguide. *Sci. Rep.* **2021**, *11*, 7978. [[CrossRef](#)] [[PubMed](#)]
38. Belt, M.; Davenport, M.L.; Bowers, J.E.; Blumenthal, D.J. Ultra-low-loss Ta₂O₅-core/SiO₂-clad planar waveguides on Si substrates. *Optica* **2017**, *4*, 532–536. [[CrossRef](#)]
39. Jung, H.; Yu, S.P.; Carlson, D.R.; Drake, T.E.; Briles, T.C.; Papp, S.B. Tantalum Kerr nonlinear integrated photonics. *Optica* **2021**, *8*, 811–817. [[CrossRef](#)]
40. Rabiei, P.; Rao, A.; Chiles, J.; Ma, J.; Fathpour, S. Low-loss and high index-contrast tantalum pentoxide microring resonators and grating couplers on silicon substrates. *Opt. Lett.* **2014**, *39*, 5379–5382. [[CrossRef](#)] [[PubMed](#)]
41. Sierra, J.H.; Rangel, R.C.; Samad, R.E.; Vieira, N.D.; Alayo, M.I.; Carvalho, D.O. Low-loss pedestal Ta₂O₅ nonlinear optical waveguides. *Opt. Express* **2019**, *27*, 37516–37521. [[CrossRef](#)]
42. Lamee, K.F.; Carlson, D.R.; Newman, Z.L.; Yu, S.P.; Papp, S.B. Nanophotonic tantalum waveguides for supercontinuum generation pumped at 1560 nm. *Opt. Lett.* **2020**, *45*, 4192–4195. [[CrossRef](#)]
43. Black, J.A.; Streater, R.; Lamee, K.F.; Carlson, D.R.; Yu, S.P.; Papp, S.B. Group-velocity-dispersion engineering of tantalum integrated photonics. *Opt. Lett.* **2021**, *46*, 817–820. [[CrossRef](#)]
44. Woods, J.R.C.; Daykin, J.; Tong, A.S.K.; Lacava, C.; Petropoulos, P.; Tropper, A.C.; Horak, P.; Wilkinson, J.S.; Apostolopoulos, V. Supercontinuum generation in tantalum pentoxide waveguides for pump wavelengths in the 900 nm to 1500 nm spectral region. *Opt. Express* **2020**, *28*, 32173–32183. [[CrossRef](#)] [[PubMed](#)]
45. Jafari, Z.; Wang, J.; Guo, Y.; Yang, M.; Zarifkar, A.; Liu, H.; Li, G.; Zhang, L. Efficient supercontinuum generation enabled by dispersion engineering in a dual-core waveguide. *Opt. Commun.* **2020**, *457*, 124664. [[CrossRef](#)]
46. Shen, J.; Yuan, J.; Cheng, Y.; Mei, C.; Lai, J.; Zhou, X.; Wu, Q.; Yan, B.; Wang, K.; Yu, C.; et al. Highly coherent mid-infrared supercontinuum generation in a strip titanium dioxide waveguide with three zero-dispersion wavelengths. *Opt. Eng.* **2022**, *61*, 117104. [[CrossRef](#)]
47. Ryu, H.; Kim, J.; Jhon, Y.M.; Lee, S.; Park, N. Effect of index contrasts in the wide spectral range control of slot waveguide dispersion. *Opt. Express* **2012**, *20*, 13189–13194. [[CrossRef](#)] [[PubMed](#)]
48. Hammani, K.; Markey, L.; Lamy, M.; Kibler, B.; Arocas, J.; Fatome, J.; Dereux, A.; Weeber, J.C.; Finot, C. Octave Spanning supercontinuum in Titanium Dioxide Waveguides. *Appl. Sci.* **2018**, *8*, 543. [[CrossRef](#)]
49. Evans, C.C.; Shtyrkova, K.; Bradley, J.D.B.; Reshef, O.; Ippen, E.; Mazur, E. Spectral broadening in anatase titanium dioxide waveguides at telecommunication and near-visible wavelengths. *Opt. Express* **2013**, *21*, 18582–18591. [[CrossRef](#)]
50. Gai, X.; Han, T.; Prasad, A.; Madden, S.; Choi, D.Y.; Wang, R.; Bulla, D.; Luther-Davies, B. Progress in Optical Waveguides Fabricated from Chalcogenide Glass. *Opt. Express* **2010**, *18*, 26635–26646. [[CrossRef](#)] [[PubMed](#)]
51. Gai, X.; Choi, D.Y.; Madden, S.; Yang, Z.; Wang, R.; Luther-Davies, B. Supercontinuum generation in the mid-infrared from a dispersion-engineered As₂S₃ glass rib waveguide. *Opt. Lett.* **2012**, *37*, 3870–3872. [[CrossRef](#)] [[PubMed](#)]
52. Hwang, J.; Kim, D.G.; Han, S. Supercontinuum generation in As₂S₃ waveguides fabricated without direct etching. *Opt. Lett.* **2021**, *46*, 2413–2416. [[CrossRef](#)]
53. Lamont, M.R.E.; Luther-Davies, B.; Choi, D.Y. Supercontinuum generation in dispersion engineered highly nonlinear ($\gamma = 10/W/m$) As₂S₃ chalcogenide planar waveguide. *Opt. Express* **2008**, *16*, 14938–14944. [[CrossRef](#)]
54. Bulla, D.A.P.; Wang, R.; Prasad, A.; Rode, A.V.; Madden, S.J.; Luther-Davies, B. On the properties and stability of thermally evaporated Ge-As-Se thin films. *Appl. Phys. A Mater. Sci. Process.* **2009**, *96*, 615–625. [[CrossRef](#)]
55. Su, X.; Wang, R.; Luther-Davies, B.; Wang, L. The dependence of photosensitivity on composition for thin films of Ge_xAs_ySe_{1-x-y} chalcogenide glasses. *Appl. Phys. A* **2013**, *113*, 575–581. [[CrossRef](#)]
56. Gai, X.; Choi, D.Y.; Madden, S. Polarization-independent chalcogenide glass nanowires with anomalous dispersion for all-optical processing. *Opt. Express* **2012**, *20*, 13513–13521. [[CrossRef](#)] [[PubMed](#)]
57. Gai, X.; Madden, S.; Choi, D.Y. Dispersion engineered Ge_{11.5}As₂₄Se_{64.5} nanowires with a nonlinear parameter of 136 W⁻¹m⁻¹ at 1550 nm. *Opt. Express* **2010**, *18*, 18866–18874. [[CrossRef](#)] [[PubMed](#)]
58. Shang, H.; Zhang, M.; Sun, D. Optical investigation of chalcogenide glass for on-chip integrated devices. *Results Phys.* **2021**, *28*, 104552. [[CrossRef](#)]

59. Shang, H.; Sun, D.; Zhang, M. On-chip detector based on supercontinuum generation in chalcogenide waveguide. *J. Light Technol.* **2021**, *39*, 3890–3895. [[CrossRef](#)]
60. Piran, S.; Noori, M.; Hashemi, S.A.S. Super-Continuum Generation in Graphene-Based Chalcogenide Slot Waveguide. *Ann. Phys.* **2022**, *534*, 2100226. [[CrossRef](#)]
61. Tremblay, J.É.; Malinowski, M.; Richardson, K.A. Picojoule-level octave-spanning supercontinuum generation in chalcogenide waveguides. *Opt. Express* **2018**, *26*, 21358–21363. [[CrossRef](#)]
62. Choi, J.W.; Han, Z.; Sohn, B.U. Nonlinear characterization of GeSbS chalcogenide glass waveguides. *Sci. Rep.* **2016**, *6*, 39234. [[CrossRef](#)]
63. Du, Q.; Luo, Z.; Zhong, H. Chip-scale broadband spectroscopic chemical sensing using an integrated supercontinuum source in a chalcogenide glass waveguide. *Photonics Res.* **2018**, *6*, 506–510. [[CrossRef](#)]
64. Krogstad, M.R.; Ahn, S.; Park, W. Optical characterization of chalcogenide Ge–Sb–Se waveguides at telecom wavelengths. *IEEE Photonics Technol. Lett.* **2016**, *28*, 2720–2723. [[CrossRef](#)]
65. Chiles, J.; Fathpour, S. Mid-Infrared Integrated Waveguide Modulators Based on Silicon-on-Lithium-Niobate Photonics. *Optica* **2014**, *1*, 350–355. [[CrossRef](#)]
66. Mayer, A.S.; Phillips, C.R.; Langrock, C.; Klenner, A.; Johnson, A.R.; Luke, K.; Okawachi, Y.; Lipson, M.; Gaeta, A.L.; Fejer, M.M. Offset-Free Gigahertz Midinfrared Frequency Comb Based on Optical Parametric Amplification in a Periodically Poled Lithium Niobate Waveguide. *Phys. Rev. Appl.* **2016**, *6*, 054009. [[CrossRef](#)]
67. Hwang, A.Y.; Stokowski, H.S.; Park, T.; Jankowski, M.; McKenna, T.P.; Langrock, C.; Mishra, J.; Ansari, V.; Fejer, M.M.; Safavi-Naeini, A.H. Mid-Infrared Spectroscopy with a Broadly Tunable Thin-Film Lithium Niobate Optical Parametric Oscillator. *Optica* **2023**, *10*, 1535–1542. [[CrossRef](#)]
68. Yu, M.; Desiatov, B.; Okawachi, Y.; Gaeta, A.L.; Lončar, M. Coherent Two-Octave-Spanning Supercontinuum Generation in Lithium-Niobate Waveguides. *Opt. Lett.* **2019**, *44*, 1222–1225. [[CrossRef](#)]
69. Guo, H.; Zeng, X.; Zhou, B.; Bache, M. Few-Cycle Solitons and Supercontinuum Generation with Cascaded Quadratic Nonlinearities in Unpoled Lithium Niobate Ridge Waveguides. *Opt. Lett.* **2014**, *39*, 1105–1108. [[CrossRef](#)]
70. Jia, J.; Kang, Z.; Huang, Q.; He, S. Mid-Infrared Highly Efficient, Broadband, and Flattened Dispersive Wave Generation via Dual-Coupled Thin-Film Lithium-Niobate-on-Insulator Waveguide. *Appl. Sci.* **2022**, *12*, 9130. [[CrossRef](#)]
71. Lu, J.; Surya, J.B.; Liu, X.; Xu, Y.; Tang, H.X. Octave-Spanning Supercontinuum Generation in Nanoscale Lithium Niobate Waveguides. *Opt. Lett.* **2019**, *44*, 1492–1495. [[CrossRef](#)]
72. Wu, T.H.; Ledezma, L.; Fredrick, C.; Sekhar, P.; Sekine, R.; Guo, Q.; Briggs, R.M.; Marandi, A.; Diddams, S.A. Visible-to-Ultraviolet Frequency Comb Generation in Lithium Niobate Nanophotonic Waveguides. *Nat. Photonics* **2024**, *18*, 218–223. [[CrossRef](#)]
73. Yu, M.; Shao, L.; Okawachi, Y.; Gaeta, A.L.; Loncar, M. Ultraviolet to Mid-Infrared Supercontinuum Generation in Lithium-Niobate Waveguides. In Proceedings of the Conference on Lasers and Electro-Optics, Washington, DC, USA, 10–15 May 2020; Optica Publishing Group: Washington, DC, USA, 2020; p. STu4H.1.
74. Jankowski, M.; Langrock, C.; Desiatov, B.; Marandi, A.; Wang, C.; Zhang, M.; Phillips, C.R.; Lončar, M.; Fejer, M.M. Ultrabroadband Nonlinear Optics in Nanophotonic Periodically Poled Lithium Niobate Waveguides. *Optica* **2020**, *7*, 40–46. [[CrossRef](#)]
75. Phillips, C.R.; Langrock, C.; Pelc, J.S.; Fejer, M.M.; Jiang, J.; Fermann, M.E.; Hartl, I. Supercontinuum Generation in Quasi-Phase-Matched LiNbO₃ Waveguide Pumped by a Tm-Doped Fiber Laser System. *Opt. Lett.* **2011**, *36*, 3912–3914. [[CrossRef](#)]
76. Reig Escalé, M.; Kaufmann, F.; Jiang, H.; Pohl, D.; Grange, R. Generation of 280 THz-Spanning near-Ultraviolet Light in Lithium Niobate-on-Insulator Waveguides with Sub-100 pJ Pulses. *APL Photonics* **2020**, *5*, 121301. [[CrossRef](#)]
77. Guo, H.; Zhou, B.; Steinert, M.; Setzpfandt, F.; Pertsch, T.; Chung, H.; Chen, Y.-H.; Bache, M. Supercontinuum Generation in Quadratic Nonlinear Waveguides without Quasi-Phase Matching. *Opt. Lett.* **2015**, *40*, 629–632. [[CrossRef](#)] [[PubMed](#)]
78. Grayson, M.; Xu, B.; Shanavas, T.; Zoharabi, M.; Bae, K.; Gopinath, J.T.; Park, W. Fabrication and characterization of high quality GeSbSe reflowed and etched ring resonators. *Opt. Express* **2022**, *30*, 31107–31121. [[CrossRef](#)] [[PubMed](#)]
79. Yan, Z.; Yan, K.; Wei, T.; Sun, Y.; Xu, P.; Madden, S.; Wang, R. Real time change of optical losses in chalcogenide waveguides induced by light illumination. *Opt. Lett.* **2022**, *47*, 5565–5568.
80. Ko, K.; Suk, D.; Kim, D.; Park, S.; Sen, B.; Wang, Y.; Dai, S.; Wang, X.; Chun, B.J.; Ko, K.; et al. The first mid-IR Brillouin laser using ultra-high Q on-chip resonator. *Nat. Photonics*, 2024; submitted.

Disclaimer/Publisher’s Note: The statements, opinions and data contained in all publications are solely those of the individual author(s) and contributor(s) and not of MDPI and/or the editor(s). MDPI and/or the editor(s) disclaim responsibility for any injury to people or property resulting from any ideas, methods, instructions or products referred to in the content.